Framework to Assess Effects of Structural Flexibility on Dynamic Loads Developed in Maneuvering Aircraft

Darshan Sarojini* , Ruxandra Duca* , Heriberto D. Solano* , Imon Chakraborty†

Simon Briceno‡ , Dimitri N. Mavris§

Aerospace Systems Design Laboratory,Georgia Institute of Technology, Atlanta, Georgia, 30332-0150

Sizing loads for major aircraft structural components are often experienced during dynamic maneuvers, several of which are described within the Federal Aviation Regulations as part of certification requirements. A simulation and analysis framework that permits such dynamic loads to be assessed earlier in the design process is an advantage for designers and aligned with the trend towards certification by analysis. Such a framework is demonstrated in this paper using the case of a business jet performing a longitudinal checked pitch maneuver. The maneuver is simulated with a six degree-of-freedom MATLAB/Simulink simulation model, using the aircraft aerodynamic characteristics, mass properties, and an adequate level of modeling for the flight control system and pilot control action. The effects of structural flexibility and deformation of the lifting surfaces and fuselage under maneuver loads are modeled by tracking a number of structural degrees-of-freedom for each. The modular nature of the simulation setup facilitates the assessment of multiple maneuvers, analysis of sensitivity to uncertainty, as well as the identification of the impact of structural flexibility through flexible versus rigid maneuver simulations.

I. Introduction

Dynamic maneuvers, in which the motion of the aircraft contributes significantly to the developed aerodynamic and inertial loads, often yield the critical or sizing loads for major aircraft components (e.g., wings, horizontal stabilizer, and vertical stabilizer). The consequences of large, unforeseen dynamic loads may be catastrophic, as evidenced by the in-flight failure of the vertical stabilizer of American Airlines Flight 587 (an Airbus A300B4 aircraft), which resulted in the loss of all on-board as well as fatalities on the ground. It was determined that the vertical stabilizer failed when the dynamic loads developed on it due to the first officer's rapid, aggressive, and oscillatory rudder inputs in response to a wake turbulence encounter exceeded its ultimate design load limits [1].

Airworthiness requirements related to structural loads and integrity can, therefore, drive the design and sizing of structural components. Compliance must be demonstrated through a combination of computational analyses and physical testing in order to establish the vehicle as being safe, durable, and reliable [2, 3]. Flight testing to ensure compliance imposes a considerable burden on the manufacturer in terms of both time and cost, and any re-design or mitigation actions necessitated in this phase can result in programmatic delays. The ability to computationally simulate and assess the structural loads arising from complex, dynamic maneuvers is, therefore, a key enabler. With appropriate fidelity, simulation-based approaches can facilitate Certification by Analysis through the simulation and evaluation of a large number of scenarios (which may be either too numerous or too risky to be attempted during actual flight testing), thus helping to de-risk the aircraft's certification program. This forms the over-arching goal of this current work.

In the United States, certification and airworthiness standards for transport category aircraft, including those pertaining to structural loads, are described in Part 25 of Title 14 of the Code of Federal Regulations

*Graduate Research Associate, ASDL, School of Aerospace Engineering, Georgia Tech, AIAA Student Member
†Research Engineer II, ASDL, School of Aerospace Engineering, Georgia Tech, AIAA Member
‡Senior Research Engineer, ASDL, School of Aerospace Engineering, Georgia Tech, AIAA Senior Member
§S.P. Langley Distinguished Regents Professor and Director of ASDL, Georgia Tech, AIAA Fellow

(14 CFR Part 25). The regulatory entity for this is the Federal Aviation Administration (FAA), and the regulations are commonly called the Federal Aviation Regulations (FARs) [4]. The capabilities developed in this work are demonstrated with reference to two specific FARs: (i) FAR §25.331(c)(2), commonly known as the *Checked Pitch Maneuver* and (ii) FAR §25.351, commonly referred to as the *Rudder Kick Maneuver*.

In prior work by the authors [5], a three degree-of-freedom (3-DoF) aircraft simulation capability was developed in order to assess dynamic loads developed on the horizontal stabilizer during the *Checked Pitch Maneuver*, in accordance with the pilot actions and test envelope specified in FAR $ 25.331(c)(2). In follow-on work [6], the sensitivity of these loads to uncertainties in the aircraft aerodynamic characteristics and mass properties was assessed.

In this work, the above-mentioned capabilities were significantly improved to enhance the fidelity and applicability of the simulation framework. The most substantial enhancement pertains to the explicit consideration of the structural dynamics. Given the increasing flexibility of modern aircraft structures, and especially for flight or maneuver conditions when large aerodynamic and inertial loads may develop, it is necessary to explicitly consider the impact of structural deformations. For established tools such as NASTRAN [7], separate structural and aerodynamic analyses are typically coupled through the use of influence matrices [8, 9]. Forced response and flutter analyses are pursued using a modal approach which, though effective, requires considerable effort to analyze a case. Modal analysis also linearizes the problem and cannot account for large deformations. The approach adopted here to account for structural flexibility is similar to that presented in [10–12] and involves tracking the time-evolution of structural (nodal) states in addition to the regular aircraft states. Further, the degrees-of-freedom are increased to 6-DoF in order to capture lateral/directional aircraft dynamics in addition to longitudinal dynamics.

The proposed approach is developed and tested using data corresponding to an aircraft from a business jet manufacturer's product line. The results to be presented in this paper will therefore be suitably modified or redacted where necessary in order to protect proprietary data corresponding to this aircraft's aerodynamics, mass properties, geometry, elastic characteristics, and performance envelope.

The remainder of the paper is organized as follows: Section II presents the MATLAB/Simulink simulation framework. Section III presents the development of the structural dynamics equation system and Section IV presents the integration of the structural dynamics with the rest of the framework. Section V presents results for trim. Section VI concludes the paper.

II. Overview of Integrated Simulation Framework

The closed-loop simulation of the aircraft and structural dynamics is done through suitable extensions to a MATLAB/Simulink flight simulation capability [5, 6], which is described in the following sections.

II.A. MATLAB/Simulink Flight Simulation Environment

Figure 1 shows the top-level of the Simulink flight simulation model. The *Maneuver* block contains Simulink elements that translate the language of the FARs of interest into corresponding actionable desired states or control inputs. The setup of this block, therefore, depends on the specific FAR being simulated. The *Pilot Controls* block contains the model of the human test pilot. Depending on the requirements of the specific FAR and the feedback of the current aircraft states, this block simulates the control actions of the pilot and generates corresponding control inputs.

The *Aircraft Dynamics* block is a complex block that contains the aerodynamic, propulsion, and structural dynamics modeling of the aircraft. The outputs from this block are the net external forces and moments on the aircraft, and structural states of each node. This information is used by the *EoM Integration* block to compute the time-evolution of the aircraft states by integrating the Equations of Motion (EoM).

The *FlightGear Interface* block interfaces the Simulink model with FlightGear Flight Simulator (FGFS) [13], generating a visual rendering of the aircraft's trajectory and motion within the FGFS environment. The customizable *Monitoring Station* block contains animated instruments (from Simulink *Aerospace Blockset*) and readouts of any aircraft parameters of interest. The *FlightGear Interface* and *Monitoring Station* blocks are used strictly to inspect the evolution of the simulation in real-time. They are deactivated (using the *FGEnable* and *MSEnable* flags respectively) when the simulation model is run in batch-mode.

The parameters required to initialize the Simulink model (e.g., vehicle aerodynamic characteristics and mass properties, trim solutions, etc.) are computed using MATLAB pre-processing scripts. Similarly, after

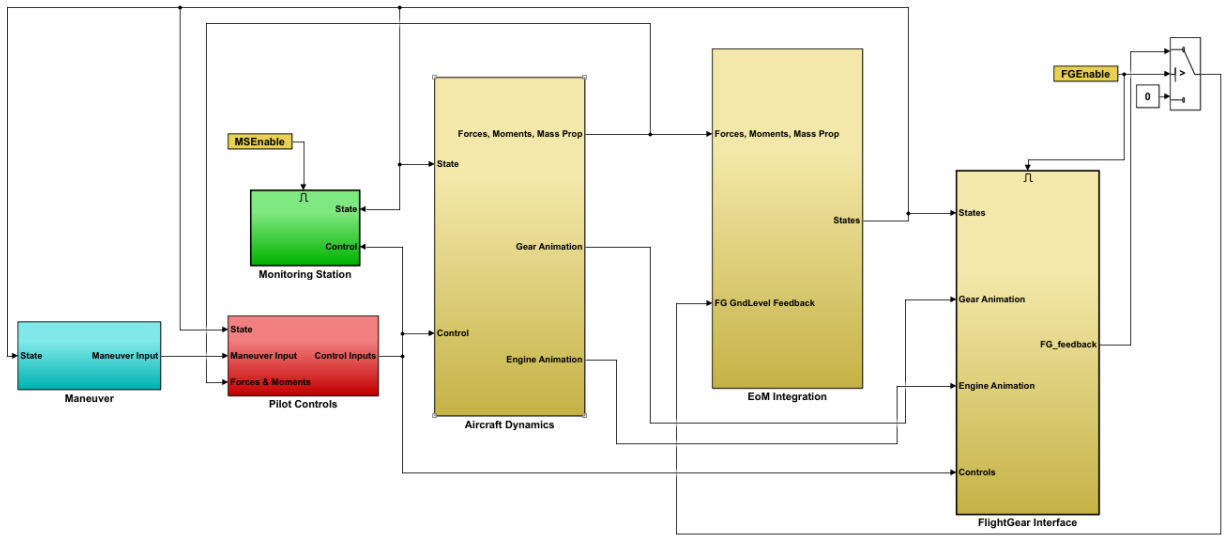

Figure 1: Top-level of Simulink model (Simulink 9.0 / MATLAB R2017b)

the simulation has completed, MATLAB post-processing scripts are used to process, query, and modify the generated data. At present, the MATLAB/Simulink model is implemented in MATLAB version R2017b. The *Structural Dynamics* block and the *Aerodynamic Build-up* are explained in-depth in this paper. The other blocks are briefly touched upon for completeness. Further details regarding the model can be found in Goron et. al. [5].

II.B. Maneuver Synthesis, Pilot Model and Flight Control System

The checked pitch maneuver is described in FAR §25.331(c)(2) in terms of the control deflection required as a function of time, the load factor, and the permissible pilot force. Starting from steady, level, flight between V_A (maneuver speed) and V_D (design dive speed), the maneuver is commenced with a target control application of a sinusoidal nature, given by

$$\delta(t) = \delta_{av} \sin(\omega t), \quad \text{for} \quad 0 \leq t \leq \frac{3\pi}{2\omega} \quad \text{and} \quad \omega \leq \frac{\pi V}{2V_A}. \tag{1}$$

To simulate the actions of a human pilot trying to match the FAR-prescribed control input, a proportional-integral-derivative (PID) controller is used. If the FAR in question requires a particular, prescribed control motion, then the error is defined as the difference between the actual and prescribed control deflections, $e(t) = \delta_{cs}(t) - \delta_{cs,ref}(t)$. If the FAR requires that a certain state be held constant or tracked (e.g., wings-level flight), then the error is defined as the difference between the actual state and the reference state, $e(t) = \hat{x}(t) - \hat{x}_{ref}(t)$. The output force is bounded within the permissible ranges specified in FAR §25.397(c). The pilot model is capable of tracking either (a) a prescribed control motion or (b) responding to the evolution of aircraft state. The pilot model outputs a force F_{pilot} to minimize the error between the target and actual control application. The maximum available displacement of the flight deck pitch control δ_{av} may be limited by the flight control system ($\delta_{av} = |\delta_{max} - \delta_{e,trim}|$) or by pilot effort in accordance with FAR §25.397(b), both of which are taken into account. The circular frequency ω is taken equal to the undamped natural frequency of the short period rigid mode of the airplane.

The amplitude δ_{av} is iteratively scaled to the extent necessary to ensure that a threshold load factor is met but not exceeded (2.5 g for nose-up maneuvers and 0 g for nose-down maneuvers). If the airplane response to this control application does not achieve the prescribed limit load factors, then the control is held for the duration required to achieve the target load factor, but not in excess of five seconds.

The pilot's yoke and rudder pedal control inputs are related to the corresponding deflections of the primary flight control surfaces (ailerons, elevators, and rudder) through a simplified model of the flight control system dynamics. For each control axis, the normalized cockpit control input $x_{cc} \in [-1, 1]$ is assumed to be related

to the control surface deflection $\delta_{cs} \in [\delta_{cs,min}, \delta_{cs,max}]$ through a constant gearing ratio G. The control effort F_{pilot} applied by the pilot is assumed to be amplified by the action of hydraulic actuators by a gain factor k. The governing equations for the flight control system are given by

$$
\begin{aligned}
m_t \ddot{x}_{cs} &= F_{pilot} - F_C - c_\ell \dot{x}_{cs} && (2)\\
I_{cs}\ \ddot{\delta}_{cs} &= M_C + H_{cs} - c_r\ \dot{\delta}_{cs} && (3)\\
M_C\ G &= (1+k)\ F_C && (4)\\
G &= \frac{\delta_{cs}}{x_{cc}} = \frac{\dot{\delta}_{cs}}{\dot{x}_{cc}} = \frac{\ddot{\delta}_{cs}}{\ddot{x}_{cc}} && (5)
\end{aligned}
$$

Equation 2 is a force balance applied to the translating elements of the control system of effective mass m_t, with c_ℓ used to model friction losses. Equation 3 is a moment balance applied to the control surface hinge line, with I_{cs} the control surface moment of inertia and H_{cs} the aerodynamic hinge moment about the hinge line, and c_r is used to model rotational friction losses. Equation 4 relates the control system force F_C, moment M_C, and gearing ratio G. The latter relates cockpit control movements to control surface deflections as per Equation 5. Combining the above yields a second-order ordinary differential equation for the control surface motion:

$$
\left[I_{cs} + \frac{m_t(1+k)}{G^2}\right]\ddot{\delta}_{cs} + \left[c_r + \frac{c_\ell(1+k)}{G^2}\right]\dot{\delta}_{cs} = F_{pilot}\left[\frac{1+k}{G}\right] + H_{cs} \qquad (6)
$$

The programming of pilot control actions is somewhat dependent on the specific FAR being assessed, and may require the evaluation of several possible branching cases.

II.C. 6-DoF Equations of Motion (within *EoM Integration* Block)

The equations of motion are written with respect to a fixed reference point O rather than the center-of-gravity (CG). This enables, for instance, the dynamics of a moving CG (e.g., due to decreasing fuel mass or fuel transfer) to be modeled. The force and moment equations in vector form are given below.

$$
\begin{aligned}
\vec{F}_{tot} &= m\left(\dot{\vec{V}}_0 + \vec{\Omega}\times\vec{V}_0 + \ddot{\vec{r}}_{oc} + \dot{\vec{\Omega}}\times\vec{r}_{oc} + 2\,\vec{\Omega}\times\dot{\vec{r}}_{oc} + \vec{\Omega}\times(\vec{\Omega}\times\vec{r}_{oc})\right),\\
\vec{M}_{o,tot} &= \bar{\bar{I}}_o\dot{\vec{\Omega}} + \vec{\Omega}\times\bar{\bar{I}}_o\ \Omega + m\ \vec{r}_{oc}\times\left(\dot{\vec{V}}_0 + \vec{\Omega}\times\vec{V}_0\right), \qquad (7)
\end{aligned}
$$

where m is the vehicle mass, $\bar{\bar{I}}_o$ the inertia tensor computed with respect to reference point O, $\vec{V}_0 = \{U,V,W\}^T$ is the velocity of the reference point O and $\vec{\Omega} = \{P,Q,R\}^T$ is the angular velocity of the aircraft. The position of the CG with respect to the reference point O is given by $\vec{r}_{oc}$. The special case of a non-moving CG coinciding with the reference point O is obtained by setting $\vec{r}_{oc} = \dot{\vec{r}}_{oc} = \ddot{\vec{r}}_{oc} = 0$. All tensor quantities in Equation 7 are resolved in the aircraft body-fixed basis, with x-axis aligned with the longitudinal axis pointing forward, and y-axis towards the starboard wing.

Standard kinematic relationships are used to obtain the derivatives of the Euler angles Φ, Θ, and Ψ from the angular rates P, Q, and R, and also derivatives of the position X_0, Y_0, and Z_0 of the reference point O from the velocities U, V, and W. The resulting system of 12 nonlinear ordinary differential equations (in $U,V,W,P,Q,R,\Phi,\Theta,\Psi,X_0,Y_0,Z_0$) for six degrees-of-freedom rigid body motion is numerically integrated to obtain the motion history of the aircraft during the maneuver.

II.D. Geometry and Mass Properties Definition

At the aircraft-level, the mass properties definition involves overall vehicle mass, CG location, and inertia tensor components specified for all load-outs/configurations of interest (as shown in Table 1). Given the duration of most maneuvers (order of seconds), no variation of aircraft mass due to fuel consumption is modeled, and a constant mass is assumed. The same argument applies to the aircraft inertia tensor, whose elements are computed with respect to the reference point and expressed in the body-fixed axis system.

$$
\bar{\bar{I}}_o = \begin{bmatrix} I_{xx} & I_{xy} & I_{zx} \\ I_{xy} & I_{yy} & I_{yz} \\ I_{zx} & I_{yz} & I_{zz} \end{bmatrix} \qquad (8)
$$

Table 1: Weight configurations

Config.	**Mass** (m)	**CG Loc.** ($\vec{r}_{oc}$)			**Inertia** ($\bar{\bar{I}}_o$)					
		x_{oc}	y_{oc}	z_{oc}	I_{xx}	I_{yy}	I_{zz}	I_{xy}	I_{yz}	I_{zx}
1	...	.	.	.	.	.	.	.	.	.
...	...	.	.	.	.	.	.	.	.	.
n	...	.	.	.	.	.	.	.	.	.

The lifting surfaces and the fuselage are each divided into multiple sections, and for each section, mass properties information similar to that shown in Table 1 is specified. As described subsequently, this breakdown of mass properties is used for the computation of inertial loads during maneuvers.

II.E. Propulsion System Modeling

The thrust is found by interpolation between the minimum and maximum thrust values at the given flight conditions, based on the throttle setting τ, as seen in Equation 9. The minimum and maximum thrust values are functions of altitude and Mach number and are queried from look-up tables.

$$T(\tau, h, M) = T_{min}(h, M) + \tau[T_{max}(h, M) - T_{min}(h, M)] \tag{9}$$

The moment due to thrust is also considered by assuming the thrust force parallel to the body-fixed x-axis and computing the position of the thrust application point relative to the aircraft fixed reference point.

III. Modeling of Structural Dynamics

Flexible surfaces (wings, horizontal stabilizer, vertical stabilizer, and fuselage) are represented using stick models as shown in Fig. 2. The following sections describe the governing relationships and implementation approach for this structural model.

III.A. Structural dynamics equations

The quantities tracked at each node are shown in Table 2. They include nodal positions, Euler angles, translational and angular velocities, translational and angular accelerations, and reaction forces and moments.

Table 2: Quantities tracked in steady-state and general case

Variable	**Body-fixed axes for "i"-th node**
$\vec{r}_i = \{x_i, y_i, z_i\}$	Position
$\dot{\vec{r}}_i = \vec{u}_i = \{u_i, v_i, w_i\}$	Nodal velocities
$\ddot{\vec{r}}_i = \dot{\vec{u}}_i$	Nodal acceleration
$\vec{\theta}_i = \{\psi, \theta, \phi\}$	Euler angles triad from body-fixed axes to csn axes
$\vec{\omega}_i = \{p_i, q_i, r_i\}$	Nodal angular rates
$\dot{\vec{\omega}}_i$	Nodal angular acceleration
$\vec{F}_i = \{F_x, F_y, F_z\}$	Force resultant
$\vec{M}_i = \{M_x, M_y, M_z\}$	Moment resultant

With a state vector defined as $X = \{\vec{r}, \vec{\theta}, \vec{F}, \vec{M}, \vec{u}, \vec{\omega}\}^T$, the governing structural equations can be written in residual form as $R(X, \dot{X}) = 0$, where the quantities in $\dot{X}$ are the time derivatives of the quantities in X. First order finite differencing can be used to relate the states to their derivatives as follows:

$$X_n = \frac{1}{t_n - t_{n-1}} X_n + \frac{-1}{t_n - t_{n-1}} X_{n-1} \tag{10}$$

For each node there are 18 variables to be solved for. If n is the number of nodes for a flexible surface, each flexible surface has $18n$ unknowns. The equations to solve the system are:

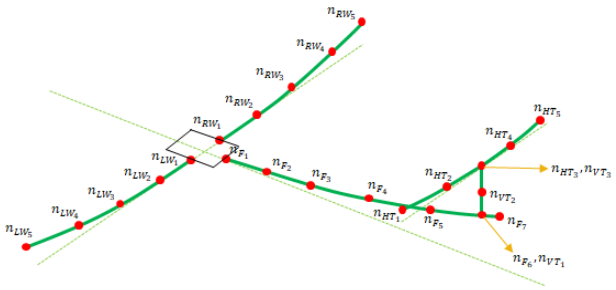

Figure 2: Aircraft stick model

1. Element equations
   (a) 3(n-1) Force equilibrium equations
   (b) 3(n-1) Moment equilibrium equations
   (c) 3(n-1) Moment-curvature relationships
   (d) 3(n-1) Strain-displacement relationships
2. Boundary conditions
   (a) 6 conditions at the root
   (b) 6 conditions at the tip
3. Nodal equations
   (a) 3n transformations: $\vec{r}_i = \vec{u}_i$
   (b) 3n transformations: $\dot{\vec{\theta}}_i = [C]\,\vec{\omega}_i$ (matrix C relates the Euler angle rates to angular velocities)

In addition, there are 12 equation-variable pairs for each "joint" in the system. Joints are used to transfer forces and moments from one beam to the other. They also enforce the constraints that the relative position and orientation between the beams (at the joint) must remain invariant. The structural dynamics formulation for this work uses nonlinear beam theory including shear deformation [10–12, 14], for which the discretized equations are presented below.

The following matrices are defined: $[T] = f\left(\vec{\theta}_i\right)$ is the transformation matrix which maps vectors the csn axes to vectors in the xyz axes, and $[K]$ is the curvature definition matrix. These matrices are different for the lifting surfaces (LS) and for the fuselage to prevent singularities in the Euler angles.

$$K_i^{LS} = \begin{bmatrix} \cos\phi\ \cos\theta & 0 & -\sin\theta \\ -\sin\phi & 1 & 0 \\ \cos\phi\ \sin\theta & 0 & \cos\theta \end{bmatrix}_i, \quad \text{and} \quad K_i^{fus} = \begin{bmatrix} \cos\theta & 0 & -\cos\psi\ \sin\theta \\ 0 & 1 & \sin\psi \\ \sin\theta & 0 & \cos\psi\ \cos\theta \end{bmatrix}_i \tag{11}$$

In the above, $[E]$ is the net moment/curvature stiffness submatrix, defined as

$$E_i = \begin{bmatrix} EI_{cc} & EI_{cs} & EI_{cn} \\ . & GJ & EI_{sn} \\ . & . & EI_{nn} \end{bmatrix}_i \tag{12}$$

The force and moment equilibrium equations in discretized form are

$$\vec{F}_{i+1} - \vec{F}_i + f_a \Delta s + \Delta\vec{F} = 0 \tag{13}$$

$$\vec{M}_{i+1} - \vec{M}_i + m_a \Delta s + \Delta\vec{M} + \Delta\vec{r} \times \vec{F}_a = 0 \tag{14}$$

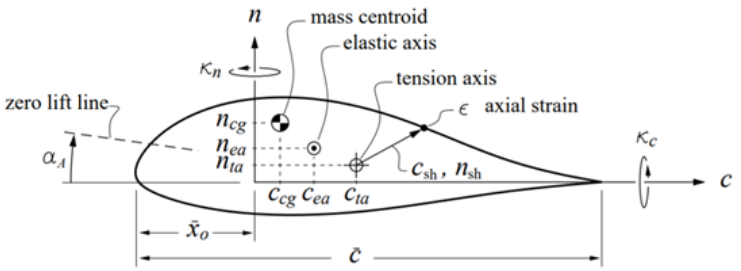

Figure 3: Cross section properties. Figure based on [10].

where $()_a$ refers to an average defined as $\frac{1}{2}\left(()_i + ()_{i+1}\right)$, and f_a and m_a are the distributed force and moment for an element. These loads comprise aerodynamic, propulsive and inertial loads. Further,

$$\vec{F}_a = \frac{1}{2}\left(\vec{F}_{i+1} + \vec{F}_i\right) \tag{15}$$

$$\vec{f}_a = f\left(\vec{\theta}, \vec{\omega}, \dot{\vec{\omega}}, \vec{r}, \vec{u}, \dot{\vec{u}}\right) \tag{16}$$

$$\vec{m}_a = f\left(\vec{\theta}, \vec{\omega}, \dot{\vec{\omega}}, \vec{r}, \vec{u}, \dot{\vec{u}}\right) \tag{17}$$

$$\Delta\vec{r} = \vec{r}_{i+1} - \vec{r}_i \tag{18}$$

$$\Delta s = (1 + \epsilon_s)\Delta s^0 \tag{19}$$

where ϵ_s is the axial strain, and Δs^0 the arc length of the element in the undeformed configuration. The inertial force and moment are calculated as

$$\vec{f}_{acc} = \mu\left(\vec{g} - \vec{a}^{cg}\right) \tag{20}$$

$$\vec{m}_{acc} = \vec{r}^{cg} \times \vec{f}_{acc} - [T]^T [i] [T]\left(\vec{\alpha}^0 + \dot{\vec{\omega}}_i\right) - \left(\vec{\Omega} + \vec{\omega}_i\right) \times \left([T]^T [i] [T]\left(\vec{\alpha}^0 + \dot{\vec{\omega}}_i\right)\right) \tag{21}$$

where μ is the mass per unit length of the element, $[i]$ the mass moment of inertia tensor per unit length, $\vec{\alpha}^0$ the acceleration of the rigid body, $\vec{\Omega}$ the aircraft rigid body angular velocity, and

$$\vec{r}^{cg} = c^{cg}\hat{c} + n^{cg}\hat{n} \tag{22}$$

$$\begin{aligned} \vec{a}_i^{cg} &= \dot{\vec{U}} + \dot{\vec{\Omega}}_{ac} \times \vec{U} + \dot{\vec{u}}_i + \dot{\vec{\Omega}}_{ac} X \vec{r}_i + \vec{\Omega}_{ac} \times \left(\vec{\Omega}_{ac} \times \vec{r}_i\right) + 2\vec{\Omega}_{ac} \times \vec{u}_i \\ &+ \left(\dot{\vec{\Omega}}_{ac} + \dot{\vec{\omega}}_i\right) \times \vec{r}_i^{cg} + \vec{\Omega}_{ac} \times \left(\vec{\Omega}_{ac} \times \vec{r}_i^{cg}\right) + \vec{\omega}_i \times (\vec{\omega}_i \times \vec{r}_i^{cg}) + 2\vec{\Omega}_{ac} \times (\vec{\omega}_i \times \vec{r}_i^{cg}) \end{aligned} \tag{23}$$

where $\vec{V}_{ac} = \{U, V, W\}^T$ is the gross aircraft velocity in body-fixed axes, $\vec{\Omega}_{ac} = \{P, Q, R\}^T$ the gross aircraft angular rates in body-fixed axes, and $\vec{r}^{cg}$ is the offset offset of the center of gravity of the section from the csn origin expressed in xyz, as shown in Fig. 3.

The moment-curvature relations for an element are

$$\frac{1}{2}\left([K]_i + [K]_{i+1}\right)\left(\vec{\theta}_{i+1}\vec{\theta}_i\right) = \frac{1}{2}\left(\left[K^0\right]_i + \left[K^0\right]_{i+1}\right)\left(\vec{\theta}^0_{i+1}\vec{\theta}^0_i\right) + \frac{\Delta s}{2}\left([E]_i + [E]_{i+1}\right)\begin{Bmatrix} M_c' \\ M_s' \\ M_n' \end{Bmatrix}_a \tag{24}$$

where

$$\begin{Bmatrix} M_c^{'} \\ M_s^{'} \\ M_n^{'} \end{Bmatrix}_a = \frac{1}{2}\left([T]_i \vec{M}_i + [T]_{i+1} \vec{M}_{i+1}\right) + \frac{1}{2}\left([D]_i [T]_i \vec{F}_i + [D]_{i+1} [T]_{i+1} \vec{F}_{i+1}\right) \tag{25}$$

$$D_i = \begin{bmatrix} 0 & -n_{ea} & 0 \\ n_{ta} & 0 & -c_{ta} \\ 0 & c_{ea} & 0 \end{bmatrix}_i, D_{i+1} = \begin{bmatrix} 0 & -n_{ea} & 0 \\ n_{ta} & 0 & -c_{ta} \\ 0 & c_{ea} & 0 \end{bmatrix}_{i+1} \tag{26}$$

$$[K]_i = f\left(\vec{\theta}_i\right), [K]_{i+1} = f\left(\vec{\theta}_{i+1}\right) \tag{27}$$

$$[T]_i = f\left(\vec{\theta}_i\right), [T]_{i+1} = f\left(\vec{\theta}_{i+1}\right) \tag{28}$$

The strain-displacement relations for an element are

$$\vec{r}_{i+1} - \vec{r}_i = \Delta s^0 \left(\frac{1}{2}[T]_{i+1} + [T]_i\right)\left[\begin{Bmatrix} 0 \\ 1 \\ 0 \end{Bmatrix} + \left(\begin{bmatrix} \frac{1}{GK_c} & 0 & 0 \\ 0 & \frac{1}{EA} & 0 \\ 0 & 0 & \frac{1}{GK_n} \end{bmatrix}[T]\vec{F}\right)_a + \left([D^T]\left[E^{-1}\right]\begin{Bmatrix} M_c^{'} \\ M_s^{'} \\ M_n^{'} \end{Bmatrix}\right)_a\right] \tag{29}$$

where GK_c and FK_n are the shear rigidities, and EA the axial stiffness.

III.B. Joints

In addition to the change of boundary conditions, to enable the definition of joints between beams, several changes were made within the dynamic equations to accommodate joints. To make such changes, a structure was created using the joint definition that allows the program to distinguish between fixed-free beams, namely "parent" parts such as the fuselage, and free-free beams or "children" parts such as the wings or tail. In the latter beams, the joint dictates the displacement of the beam. Thus, the resulting structure is shown in Figure 4.

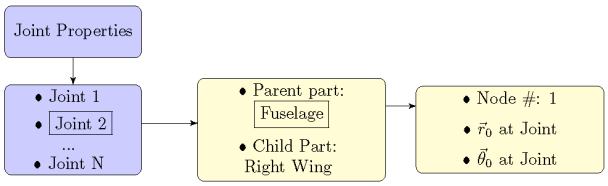

Figure 4: Joint structure definition

The structure will allow the code to traverse through the required joint positions at each of the beam elements that belong to the entire aircraft, providing the exact place at which the changes in the residuals have to occur.

With the joint definition prepared, Figure 5 illustrates the process followed inside the code to include the joints in the residual calculation for the solution of the dynamics equations.

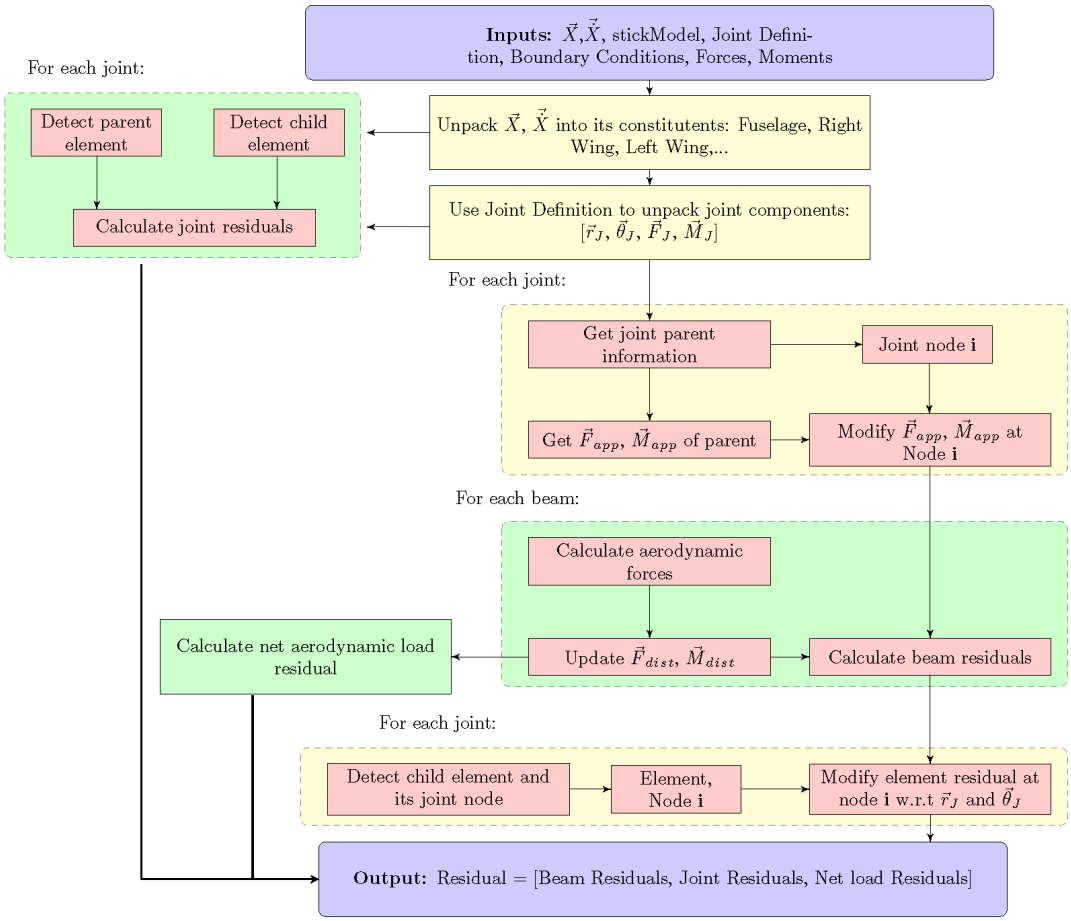

Figure 5: Structure of the residual solver

From the diagram, there are different quantities that are altered and calculated using the geometry and the state. These include:

1. The modification of the applied forces at the parent joint point (#1). For that, the joint loads are applied as concentrated loads at the node of the parent beam:

$$\Delta\vec{M}_J = \vec{M}_J \ , \ \Delta\vec{F}_J = \vec{F}_J \tag{30}$$

2. The computation of the effective angle of attack and distributed aerodynamic loads.

3. The calculation of the different beam residuals by using the structural dynamics equations.

4. The imposition of an additional position and Euler angle change kinematic constraints at the child joint point (#2). These are used instead of the force and moment balance equations (16), (17) across the joint node corresponding to the child beam:

$$\Delta\vec{r}_i = \vec{r}_{0_i} + \Delta\vec{r}_J \ , \ \Delta\vec{\theta}_i = \vec{\theta}_{0_i} + \Delta\vec{\theta}_J \tag{31}$$

5. The calculation of the net aerodynamic load residuals.

6. The calculation of the joint residuals with additional equations.

In particular, the set of 12 equations required to solve the states of the variables $\Delta\vec{r}_J$, $\Delta\vec{\theta}_J$, $\Delta\vec{M}_J$, $\Delta\vec{F}_J$ for each joint are the following:

$$\vec{r}_2 - \vec{r}_1 = [T]_1^T [T]_{1_0} (\vec{r}_{2_0} - \vec{r}_{1_0}) \tag{32}$$

$$[[T]_1^T[T]_{1_0}] \times \cdot [[T]_2^T[T]_{2_0}] = 0 \tag{33}$$

$$\vec{F}_{i+1} - \vec{F}_i + \vec{f}_a \Delta s + \Delta \vec{F} = \vec{F}_J \tag{34}$$

$$\vec{M}_{i+1} - \vec{M}_i + \vec{m}_a \Delta s + \Delta \vec{M} + \Delta \vec{r} \times \vec{F}_a = \vec{M}_J - (\vec{r}_{i_2} - \vec{r}_{i_1}) \times \vec{F}_J \tag{35}$$

In which $()_1$ and $()_2$ denote the beam variables at the parent (#1) and the child (#2) joint locations, and $()_0$ denotes the unloaded "jig" state. Eq. 32 constrains the joint element to remain at its original length, while the tensor cross-dot product in Eq. 33 constrains the two joined beams at their location to maintain the same relative orientation. Equations 34 and 35 enforce force and moment balance at the child (#2) joint respectively, which were removed to allow the six kinematic constraints shown in Eq. 31.

All the previously introduced equations are solved by constructing residuals, which are then grouped and solved by using Newton's method, but for that, a method of calculating the Jacobian is needed.

III.C. Jacobian

When the number of nodes becomes large, using finite difference to obtain the Jacobian is a computational bottleneck. Due to the nature of the formulation (using average quantities and difference between nodal quantities in the residual equations, a large number of terms in the Jacobian are identically zero. The equations were analytically differentiated to obtain closed-form analytical expressions for Jacobian elements. Matlab's *fsolve* algorithm has the functionality to accept a pre-computed Jacobian. It also performs a one-time gradient check to ensure that the given Jacobian matches the numerically computed one. The form of the Jacobian is as follows:

$$J = \begin{bmatrix} \frac{\partial Res_1|_{n_1}}{\partial r_x|_{n_1}} & \frac{\partial Res_1|_{n_1}}{\partial r_y|_{n_1}} & \cdots & \frac{\partial Res_1|_{n_1}}{\partial \omega_z|_{n_1}} & \frac{\partial Res_1|_{n_1}}{\partial r_x|_{n_2}} & \cdots & \frac{\partial Res_1|_{n_1}}{\partial \omega_z|_{n_n}} \\ \frac{\partial Res_2|_{n_1}}{\partial r_x|_{n_1}} & \frac{\partial Res_2|_{n_1}}{\partial r_y|_{n_1}} & \cdots & \frac{\partial Res_2|_{n_1}}{\partial \omega_z|_{n_1}} & \frac{\partial Res_2|_{n_1}}{\partial r_x|_{n_2}} & \cdots & \frac{\partial Res_2|_{n_1}}{\partial \omega_z|_{n_n}} \\ \vdots & \vdots & \vdots & \vdots & \vdots & \vdots & \vdots \\ \frac{\partial Res_{12}|_{n_1}}{\partial r_x|_{n_1}} & \frac{\partial Res_{12}|_{n_1}}{\partial r_y|_{n_1}} & \cdots & \frac{\partial Res_{12}|_{n_1}}{\partial \omega_z|_{n_1}} & \frac{\partial Res_{12}|_{n_1}}{\partial r_x|_{n_2}} & \cdots & \frac{\partial Res_{12}|_{n_1}}{\partial \omega_z|_{n_n}} \\ \frac{\partial Res_1|_{n_2}}{\partial r_x|_{n_1}} & \frac{\partial Res_1|_{n_2}}{\partial r_y|_{n_1}} & \cdots & \frac{\partial Res_1|_{n_2}}{\partial \omega_z|_{n_1}} & \frac{\partial Res_1|_{n_2}}{\partial r_x|_{n_2}} & \cdots & \frac{\partial Res_1|_{n_2}}{\partial \omega_z|_{n_n}} \\ \vdots & \vdots & \vdots & \vdots & \vdots & \vdots & \vdots \\ \frac{\partial Res_{12}|_{n_n}}{\partial r_x|_{n_1}} & \frac{\partial Res_{12}|_{n_n}}{\partial r_y|_{n_1}} & \cdots & \frac{\partial Res_{12}|_{n_n}}{\partial \omega_z|_{n_1}} & \frac{\partial Res_{12}|_{n_n}}{\partial r_x|_{n_2}} & \cdots & \frac{\partial Res_{12}|_{n_n}}{\partial \omega_z|_{n_n}} \end{bmatrix} \tag{36}$$

The Jacobian has a specific structure: the first 18 rows are the derivatives of 18 residual equations for the first node, rows 19 to 36 are the derivatives of 18 residual equations of node 2, and so on. The first column is the partial derivative of a residual equation wrt variable r_x at node 1. Columns 1-18 are the partial derivatives of a residual equation wrt $\vec{x}$ variables at the 1st node, columns 19-36 are the partial derivatives of a residual equation wrt $\vec{x}$ variables at the 2nd node, and so on. The Jacobian will have 18n X 18n terms in it per beam.

In the presence of joints, 6 force and moment balance equations are removed from each node and replaced with 6 kinematic constraints. Hence, the appropriate rows in the Jacobian must be modified. Further, the Jacobian must be augmented with 12 rows and columns corresponding to the 12 joint equations, for each joint. The sparse nature of the Jacobian for a case with 2 beams joined together is shown in Fig. 6.

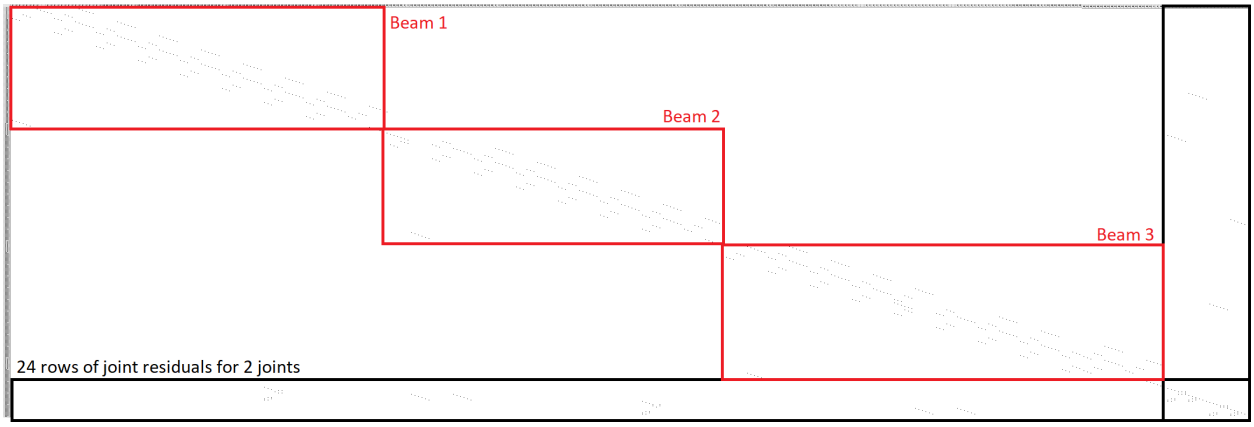

Figure 6: Sparsity of square Jacobian matrix for 3 beams with 2 joints: fuselage cantilevered, vertical tail joined to fuselage, horizontal tail joined to the vertical tail

The structural dynamics formulation in this section is agnostic to the nature of loads applied on the beams. If the loads applied are *dead loads* (which do not change in magnitude and direction due to deformation), terms in the Jacobian such as $\frac{\partial F_i}{\partial \theta_i} = 0$. Aerodynamic forces on the other hand are *follower forces* (whose magnitudes vary with the structural deformation), and hence contribute to terms in the Jacobian.

III.D. Implementation of Structural Dynamics Residual Solver

The model used in this paper is shown in Fig. 7.Note that the vertical tail is not modeled as a flexible beam. It only contributes to mass properties and drag. The fuselage is divided into two sections, a rigid front section, and a flexible rear section. The flexible rear section of the fuselage is assumed to be a fixed-free beam. The ground point is provided at the location where the leading edge of the wing meets the fuselage. The boundary conditions enforce the fact that nodal forces and moments are zero at the tip, while nodal displacement and rotations are zero at the root.

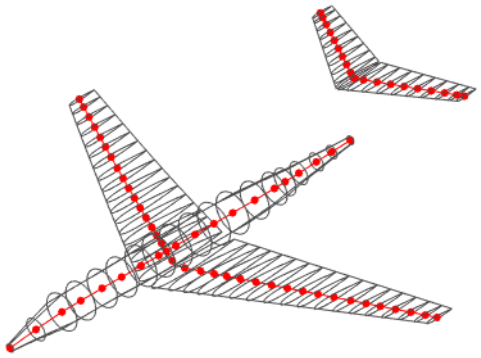
Figure 7: Isometric view of the model used in this paper

The right wing and left wing are joined to the fuselage using the joint variables. For a T-tail aircraft, the vertical tail omitted. The two halves of the horizontal tail are joined to the fuselage through a massless rigid rod. Thus, the appropriate boundary conditions for the each of these beams are free-free, as the kinematics will be constrained through the joints.

The solver will attempt to find the values of the unknowns (elements of X) by driving the residuals of non-linear system of equations to zero. To start the time marching, the states from the trim solution can be given as the initial conditions. The residual system is solved using Newton iterations. The pseudo-code for the solver is given in Algorithm 1.

Algorithm 1 Structural Dynamics Time Marching

while $t < t_{final}$ **do**
  $t = t + \Delta t$
  $\vec{x}_n = \vec{x}_{n-1}$ ▷ Guess from previous solution
  $\dot{\vec{x}}_n = 0$
  $k_0 = \frac{1}{\Delta t}$, $k_1 = -k_0$
  Convergence Flag = 0
  $\vec{x} = \vec{x}_n$, $\dot{\vec{x}} = \dot{\vec{x}}_n$ ▷ Initialize for current time step
  while Convergence Flag != 1 **do**
    function SrucDynResiduals(StickModels, $\vec{x}, \dot{\vec{x}}, \vec{F_{ext}}, \vec{M_{ext}}$, BC)
      Evaluate residuals of each stickmodel
      Modify residuals for each joint
      Evaluate joint residuals
      Combine all residuals to form residual vector $\vec{r}$
      Compute Jacobians $\frac{\partial \vec{r}}{\partial \vec{x}}$ and $\frac{\partial \vec{r}}{\partial \dot{\vec{x}}}$
      return $\vec{r}$, $\frac{\partial \vec{r}}{\partial \vec{x}}$, $\frac{\partial \vec{r}}{\partial \dot{\vec{x}}}$
    end function
    $\left[\frac{\partial \vec{r}}{\partial \vec{x}} + k_0 \frac{\partial \vec{r}}{\partial \dot{\vec{x}}}\right] \vec{\delta_x} = -\vec{r}$ ▷ Solve Linear System
    if norm($\vec{r}$)< ϵ **then**
      Convergence Flag = 1
    else
      $\vec{x} = \vec{x} + \vec{\delta_x}$ ▷ New guess for $\vec{x}$
      $\dot{\vec{x}} = k_0 \vec{x} + k_1 \vec{x}_{n-1}$
    end if
  end while
  $\vec{x}_n = \vec{x}$, $\dot{\vec{x}}_n = \dot{\vec{x}}$ ▷ Converged solution at a time step
end while

IV. Integrating Structural Flexibility in Aircraft Maneuvers

The formulation presented previously allows the variation of the structural states of each node to be obtained as a function of time. It requires mass properties as defined in Section II.D. The mass properties account for deformation due to self-weight of each structural component. The masses and mass moments of inertia are used to develop inertial loads due motion of the nodes as well as gross motion of the aircraft. Loads due to thrust are obtained as given in Section II.E. The aerodynamic build-up is given next.

IV.A. Aerodynamic loads build-up

The structural dynamics equations are expressed in aircraft body-fixed axes. Hence, the aerodynamic loads have to be ultimately converted to and applied in the same axes. The aerodynamic loads on each panel of the lifting surface are first computed in the local csn axes and then rotated to the aircraft body-fixed axes. The loads in the csn axes are written as build-ups using aerodynamic coefficients as follows:

$$\vec{F}^{csn}_{aero} = \vec{F}^{csn}_{aero,angles} + \vec{F}^{csn}_{aero,defl} \tag{37}$$

$$\vec{M}^{csn}_{aero} = \vec{M}^{csn}_{aero,angles} + \vec{M}^{csn}_{aero,defl} \tag{38}$$

where $()_{aero,angles}$ are the loads due to angle of attack α or sideslip angle β, and $()_{aero,defl}$ the incremental loads at due to deflection of control surfaces.

Each of these loads are computed by multiplying the corresponding aerodynamic coefficient with the dynamic pressure and reference area (for forces), and reference area and chord (for moments). The loads

due to angles are built-up as:

$$\vec{F}^{csn}_{aero,angles} = qA \begin{bmatrix} C^c_{n_{alpha}} + C^c_{n_{beta}} \\ C^s_{n_{alpha}} + C^s_{n_{beta}} \\ C^n_{n_{alpha}} + C^n_{n_{beta}} \end{bmatrix} \tag{39}$$

$$\vec{M}^{csn}_{aero,angles} = qAc \begin{bmatrix} C^c_{m_{alpha}} + C^c_{m_{beta}} \\ C^s_{m_{alpha}} + C^s_{m_{beta}} \\ C^n_{m_{alpha}} + C^n_{m_{beta}} \end{bmatrix} \tag{40}$$

where $()^{()}_{angles,alpha} = f(M, \alpha)$ are the aerodynamic coefficients due to effective angle of attack seen by each panel, $()^{()}_{angles,beta} = f(M, \beta)$ the aerodynamic coefficients due to effective sideslip angle seen by each panel, c the reference chord used to compute the moment coefficients, and A the reference area used to compute the force and moment coefficients. .

Table 3 gives a list of the aerodynamic coefficients used and the quantities they depend on. If additional control surfaces exist, their coefficients will have to be accounted for. Each of the aerodynamic coefficients listed in Table 3 have to be used for each component of the aircraft (wing, horizontal tail, vertical tail, fuselage, pylon, nacelle, etc.).

Table 3: Aerodynamic coefficients used in aerodynamic load build-up

Coefficient	Term	Function of
$C_{n_{alpha}}$, $C_{m_{alpha}}$	Angles	Mach number (M), effective angle of attack (α)
$C_{n_{beta}}$, $C_{m_{beta}}$	Angles	Mach number (M), effective sideslip angle (β)
$C_{n_{dElv}}$, $C_{m_{dElv}}$	Control surface deflections	Mach number (M), elevator deflection (δ_e)
$C_{n_{dAil}}$, $C_{m_{dAil}}$	Control surface deflections	Mach number (M), aileron deflection (δ_a)
$C_{n_{dRud}}$, $C_{m_{dRud}}$	Control surface deflections	Mach number (M), rudder deflection (δ_r)
$C_{n_{dSpl}}$, $C_{m_{dSpl}}$	Control surface deflections	Mach number (M), spoiler deflection (δ_{spl})
$C_{n_{dETab}}$, $C_{m_{dETab}}$	Control surface deflections	Mach number (M), elevator tab deflection (δ_{tab})

Lookup tables for all the aerodynamic coefficients representative of a business jet was used for both gross aircraft tail-off and tail-only; and on a *per panel* basis as well. These lookup tables were used to generate gridded interpolants (MATLAB: *griddedInterpolant*).

Finally, the computed aerodynamic forces were transferred to the body-fixed axes as

$$\vec{F}^{xyz}_{aero} = T^T \vec{F}^{csn}_{aero} \tag{41}$$

The above aerodynamic build-up assumed that the effective angle of attack and effective sideslip angle for each panel on a surface are known. A number of factors such as sweep, dihedral, twist, downwash, aircraft motion, and structural element motion influence the effective angles. The next section provides analytical expressions to obtain the angle.

IV.B. Computation of Effective Aerodynamic Angles

The computation of effective angles involves the computation of velocity as seen by the panel. Fig. 8 shows the sequence of transformations from the inertial axes to the point p of interest. The following terms are defined:

$\vec{V}^{+}_{ac} = \{U_{fd}, V_{fd}, W_{fd}\}^T$	Aircraft velocity, flight dynamics axes (m/s)
$\vec{\Omega}^{+}_{ac} = \{P_{fd}, Q_{fd}, R_{fd}\}^T$	Aircraft angular rates, flight dynamics axes (rad/s)
$\Delta\vec{r}_{p,i} = \{\Delta r_{p,i,x}, \Delta r_{p,i,y}, \Delta r_{p,i,z}\}^T$	Position of offset point P of i'th node, body-fixed axes (m)
$\Delta\vec{r}^{*}_{p,i} = \{\Delta r_{p,i,c}, \Delta r_{p,i,s}, \Delta r_{p,i,n}\}^T$	Position of offset point P of i'th node, *csn* axes (m)
$\vec{V}_{p,i} = \{V_{p,i,x}, V_{p,i,y}, V_{p,i,z}\}^T$	Velocity of offset point P of i'th node, body-fixed axes (m/s)
$\vec{V}^{*}_{p,i} = \{V_{p,i,c}, V_{p,i,s}, V_{p,i,n}\}^T$	Velocity of offset point P of i'th node, *csn* axes (m/s)
$\alpha_{p,i}$	Incidence angle seen at offset point P of i'th node (rad)

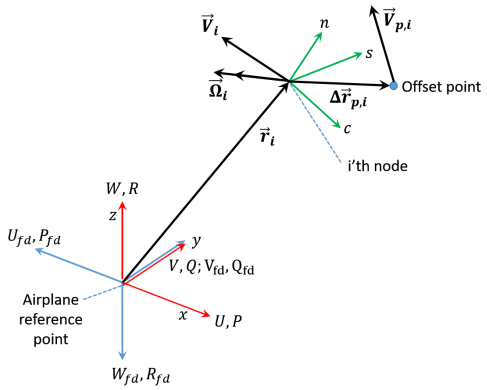

Figure 8: Sequence of transformations to obtain velocity at point p

For the case of a lifting surface, the components of an arbitrary vector $\vec{X}^*$ expressed in the *csn* axes are related to the components $\vec{X}$ in the body-fixed axes as

$$\begin{aligned} \vec{X}^* &= T\,\vec{X} \\ T &= \begin{bmatrix} c_\theta c_\psi & c_\theta s_\psi c_\phi + s_\theta s_\phi & c_\theta s_\psi s_\phi - s_\theta c_\phi \\ -s_\psi & c_\psi c_\phi & c_\psi s_\phi \\ s_\theta c_\psi & s_\theta s_\psi c_\phi - c_\theta s_\phi & s_\theta s_\psi s_\phi + c_\theta c_\phi \end{bmatrix} \end{aligned} \tag{42}$$

Using the transformation of Equation 42, the coordinates of the offset point P expressed in the *csn* axes (which are *fixed* numbers) can be related to their corresponding coordinates in the body-fixed axes:

$$\begin{aligned} \Delta r_{p,i,x} &= c_\theta c_\psi \Delta r_{p,i,c} - s_\psi \Delta r_{p,i,s} + s_\theta c_\psi \Delta r_{p,i,n} \\ \Delta r_{p,i,y} &= (c_\theta s_\psi c_\phi + s_\theta s_\phi)\Delta r_{p,i,c} + c_\psi c_\phi \Delta r_{p,i,s} + (s_\theta s_\psi c_\phi - c_\theta s_\phi)\Delta r_{p,i,n} \\ \Delta r_{p,i,z} &= (c_\theta s_\psi s_\phi - s_\theta c_\phi)\Delta r_{p,i,c} + c_\psi s_\phi \Delta r_{p,i,s} + (s_\theta s_\psi s_\phi + c_\theta c_\phi)\Delta r_{p,i,n} \end{aligned} \tag{43}$$

The inertial velocity of offset point P of the i'th node, expressed in the aircraft body-fixed basis, is given by:

$$\vec{V}_{p,i} = \vec{V}_{ac} + \vec{V}_i + \vec{\Omega}_{ac} \times \vec{r}_i + \left(\vec{\Omega}_{ac} + \vec{\Omega}_i\right) \times \Delta\vec{r}_{p,i} \tag{44}$$

The corresponding scalar equations for the three velocity components are given by:

$$\begin{aligned} V_{p,i,x} &= U + u_i - Ry_i + Qz_i - (R + r_i)\Delta r_{p,i,y} + (Q + q_i)\Delta r_{p,i,z} \\ V_{p,i,y} &= V + v_i + Rx_i - Pz_i + (R + r_i)\Delta r_{p,i,x} - (P + p_i)\Delta r_{p,i,z} \\ V_{p,i,z} &= W + w_i - Qx_i + Py_i - (Q + q_i)\Delta r_{p,i,x} + (P + p_i)\Delta r_{p,i,y} \end{aligned} \tag{45}$$

Using the transformation of Equation 42, these are converted into components along the nodal *csn* axes as

$$\begin{aligned} V_{p,i,c} &= c_\theta c_\psi V_{p,i,x} + (c_\theta s_\psi c_\phi + s_\theta s_\phi)V_{p,i,y} + (c_\theta s_\psi s_\phi - s_\theta c_\phi)V_{p,i,z} \\ V_{p,i,s} &= -s_\psi V_{p,i,x} + c_\psi c_\phi V_{p,i,y} + c_\psi s_\phi V_{p,i,z} \\ V_{p,i,n} &= s_\theta c_\psi V_{p,i,x} + (s_\theta s_\psi c_\phi - c_\theta s_\phi)V_{p,i,y} + (s_\theta s_\psi s_\phi + c_\theta c_\phi)V_{p,i,z} \end{aligned} \tag{46}$$

Regardless of the orientation of the lifting surface relative to the aircraft, the local incidence angle at the i'th node is given by

$$\alpha_i = \tan^{-1}\left(\frac{V_{p,i,n}}{V_{p,i,c}}\right) \tag{47}$$

IV.C. Aeroelastic Trim

The computation of trim involves finding the angle of attack α, sideslip angle β, throttle setting τ, and control surface deflections which result in steady-state flight. Here we restrict the control surfaces to be elevator δ_e for pitching motion, aileron δ_a for rolling motion, and rudder δ_r for yawing motion. Then, the vector being solved during trim is:

$$\vec{x}_{trim} = \{\alpha, \beta, \tau, \delta_e, \delta_a, \delta_r, \vec{x}\}^T \tag{48}$$

where $\vec{x}$ is the entire structural states vector defined in Table 2 along with any joints.

This represents 6 additional variables which require 6 equations for the system to be solved. The 6 equations required are the constraints that the aircraft is in equilibrium at a chosen reference point:

$$\begin{aligned} \sum \vec{\mathcal{F}} &= 0 \\ \sum \vec{\mathcal{M}} &= 0 \end{aligned} \tag{49}$$

IV.C.1. Implementation of Aeroelastic Trim

Enforcing the constraints in Eq. 49 involves the computation of the net forces and moments at the aircraft reference point. The structural dynamics formulation computes the reaction forces and moments at each node in every stick model. The nodal reactions at a location where a ground constraint (fixed) is provided represents the net loads on the entire beam. When joints are used, the effect of the child-beam is transfered onto the parent beam through the joint. Hence, it is sufficient to use the nodal reactions at the ground constraint of the parent beam to include the loads seen by the child beam. A pseudo-code for the trim computation is shown in Algorithm 2. FPA is the flight path angle of the aircraft.

Algorithm 2 Aeroelastic Trim Solver

Convergence Flag = 0
$\vec{x}_{trim_{guess}} = \{\alpha, \beta, \tau, \delta_e, \delta_a, \delta_r, \vec{x}\}^T$
while Convergence Flag != 1 **do**
  function AeroElasTrimResiduals(StickModels, $\vec{x}_{trim}$, BC, V_∞, Altitude, FPA)
    $\Theta = \alpha \cos\Phi + \beta \sin\Phi + FPA$ ▷ Aircraft attitude
    $U = V_\infty \cos\beta \cos\alpha, V = V_\infty \sin\beta, W = V_\infty \cos\beta \sin\alpha$ ▷ Aircraft velocities
    Compute distributed aerodynamic loads and thrust loads on each flexible beam
    Evaluate residuals of each stickmodel
    Modify residuals for each joint
    Evaluate joint residuals
    Transfer root loads of parent stickmodel to aircraft reference point
    Evaluate weights and aerodynamic loads on non-flexible surfaces at reference point
    Combine all residuals to form residual vector $\vec{r} = \{\vec{r}_{struc}, \vec{r}_{joint}, \sum \vec{\mathcal{F}}, \sum \vec{\mathcal{M}}\}$
    Compute Jacobians $\frac{\partial \vec{r}}{\partial \vec{x}}$ and $\frac{\partial \vec{r}}{\partial \dot{\vec{x}}}$
    return $\vec{r}$, $\frac{\partial \vec{r}}{\partial \vec{x}}$, $\frac{\partial \vec{r}}{\partial \dot{\vec{x}}}$
  end function
  $\left[\frac{\partial \vec{r}}{\partial \vec{x}} + k_0 \frac{\partial \vec{r}}{\partial \dot{\vec{x}}}\right] \vec{\delta_x} = -\vec{r}$ ▷ Solve Linear System
  if norm($\vec{r}$)< ϵ **then**
    Convergence Flag = 1
  else
    $\vec{x} = \vec{x} + \vec{\delta_x}$ ▷ New guess for $\vec{x}$
  end if
end while

For a setup as seen in Fig. 2, the effects of the left wing, right wing, vertical tail, left horizontal tail, and right horizontal tail are all transmitted to the flexible part of the fuselage through joints. Hence, the reaction loads at the location where the fuselage is fixed contains the net loads of all the beams joined to it.

The reaction loads at the fuselage ground location can be transferred to an aircraft reference point as

$$\vec{\mathcal{F}} = \vec{F}_{FuselageGround}$$
$$\vec{\mathcal{M}} = \vec{M}_{FuselageGround} + \vec{r}_{FuselageGround-RefPoint} \times \vec{F_{FuselageGround}} \tag{50}$$

It should be noted that the thrust loads are applied as concentrated forces on the flexible back part of the fuselage. The front of the fuselage is assumed to be rigid. Hence, its mass, and the aerodynamic forces are computed. They are appropriately transferred to the reference point. In this manner all loads (weight, thrust, aerodynamic) on the aircraft are accounted for at the reference point.

IV.D. Aeroelastic Aircraft Maneuvers

When solving for the aircraft maneuver, in addition to the structural states, the gross aircraft states defined in Table IV.D are tracked.The various stick models are defined and joints are used to relate them. The initial conditions are set using the trim solution. Algorithm 1 is used to drive the residuals of the system to zero. If the maneuver is started from a trim state, Algorithm 1 will yield zero residuals. For non-zero residuals to occur, control surfaces must be deflected to set the aircraft into a maneuver.

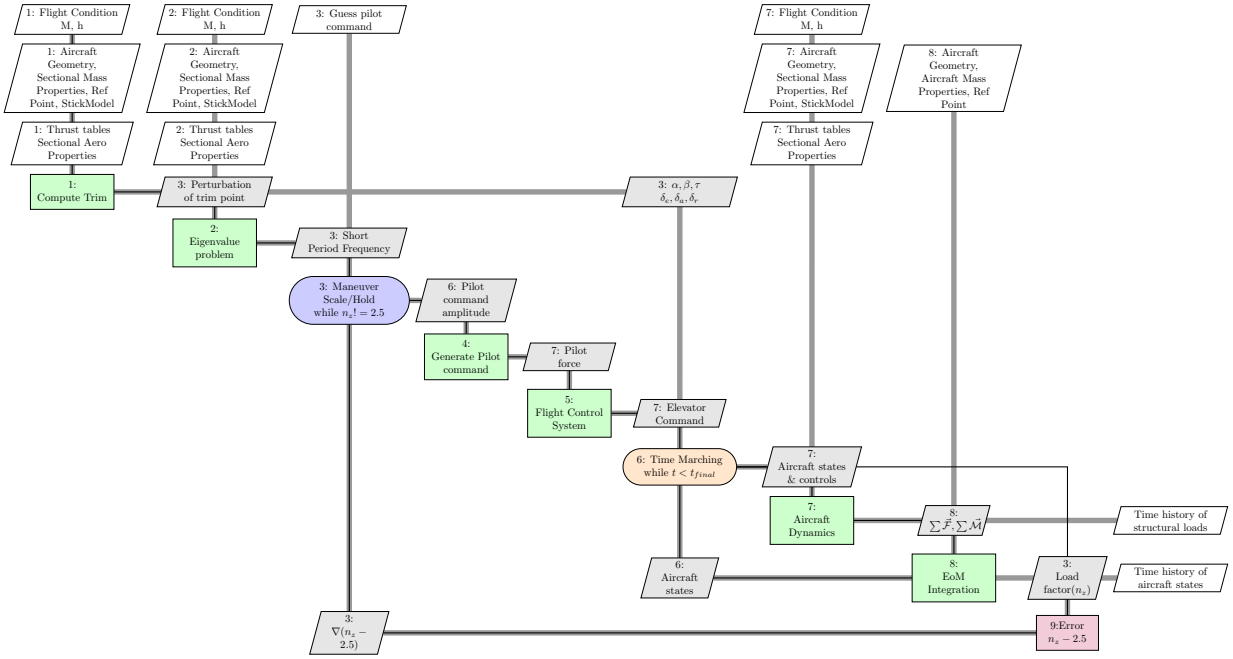

Figure 9: Checked pitch maneuver evaluation flowchart

Figure. 9 shows the entire process of simulating an FAR specified maneuver. Control surface inputs synthesized in the *Maneuver Block* shown in Fig. 1 are given to the *Aircraft Dynamics* block through the *Pilot Controls* block. The structural dynamics code developed in Section III resides within the *Aircraft Dynamics* block. The change in control surface results in different aerodynamic loads on the structure. Algorithm 1 is used to converge on the system to obtain the deformation and the net loads seen by the flexible members. The loads are transferred to the aircraft point. Loads developed on rigid members are also calculated and transferred to the aircraft reference point.

The *EoM Integration* block uses the forces and moments and integrates the flight dynamics equations of motion given by Eq. 7 to obtain the new states of the aircraft. These states are fed back into the other blocks. This process is repeated to obtain the time evolution of the aircraft and structural states.

It should be noted that the flight dynamics axes is different from the body-fixed structural axes. This involves a 180 degree rotation about the y-axis (rotating *forward-right-down* to *aft-right-up*). Thus, the signs of components along the x and z axes simply have to be reversed.

$$\begin{aligned} U &= -U_{fd}, \qquad V = V_{fd}, \qquad W = -W_{fd} \\ P &= -P_{fd}, \qquad Q = Q_{fd}, \qquad R = -R_{fd} \end{aligned} \tag{51}$$

Table 4: Aircraft states tracked during dynamic maneuver

$\vec{R_E}$	Aircraft position
$\vec{\Theta} = \{\Phi, \Theta, \Psi\}^T$	Aircraft attitude
$\vec{U} = \{U, V, W\}^T$	Aircraft velocities
$\vec{\Omega} = \{P, Q, R\}^T$	Aircraft angular velocities
$\vec{a_0}$	Aircraft acceleration
$\vec{\alpha_0}$	Aircraft angular acceleration

V. Results

V.A. Trim

Incorporating structural flexibility affects not only the maneuver and the loads time histories, but also the starting point, which is trim. The trim solution consists of angle of attack, elevator deflection, and throttle setting. These are calculated by ensuring that the forces and moments (including inertial forces and moments) add up to zero for the given flight condition. They depend on the aerodynamic loads, which in turn depend on the shape of the fuselage and lifting surfaces, and vice versa. Therefore, a different trim solution will result when the structure is allowed to deform until aeroelastic convergence is achieved.

When comparing a single case the one that resulted in critical loads in the rigid formulation the following trends are observed in Figure 10.

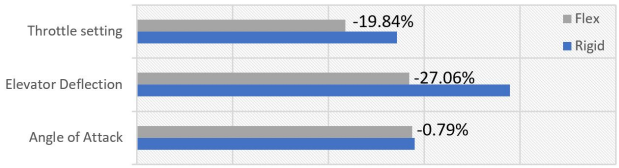

Figure 10: Rigid and flexible trim solution for reference case

For this high dynamic pressure case, there is little change in the angle of attack required for trim (<1% relative change when flexibility is added). However, there are significant reductions in the elevator deflection (∼27%) and throttle setting (∼20%). To understand how these trends vary over multiple flight conditions, the trim solution was calculated for a range of Mach numbers from around 0.45 up to over 0.90, all for the same altitude.

As seen in Figure 11a The relative differences in the angles of attack were consistently under 6%, with the exception of the high Mach number cases where the aircraft was close to its dive speed. When flexibility was considered, the angle of attack required was smaller at lower speeds and higher at high speeds. The reference case discussed above is the middle case in this graph.

Figure 11b shows the same type of comparison for the elevator deflection. In this case, the differences are more significant, especially at lower speeds. Lastly, in the case of throttle, adding flexibility showed a reduction in the throttle setting required for trim for all cases except the one close to dive. The relative change was between 15-20% for the entire range of Mach numbers. Figure 11c shows these results.

Overall, the changes in the trim solutions are not negligible and further enforce the need to consider flexibility when creating this type of simulation. Doing so results in more accurate and realistic results, that can better predict real scenarios such as flight tests.

V.B. Static Sizing Conditions

The aircraft wing is typically sized due to loads at -1g and 2.5g. The framework was used to solve for the trim state at these loading conditions. Fig. 12a gives a comparison of the jig shape, and the deflected shape of the wing at different g's. As expected, at positive g's, the wing deflects upwards with the deflection being greater for 2.5g than for 1g. The wing deflects downward for -1g. The 2.5g and -1g produce the most severe loads on the wing. The horizontal tail on the other hand (Fig. 12b) produces downward force to trim the aircraft. Hence, the deflection is downward. The -1g case produced the most severe load on the HT. Fig. 13

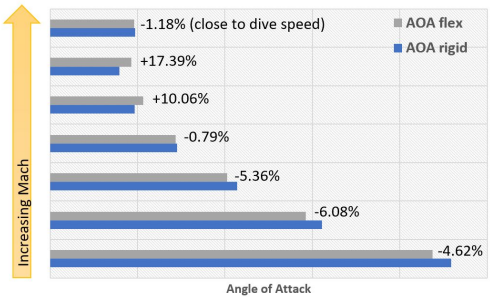

(a) Trim angle of attack as a variation of Mach number

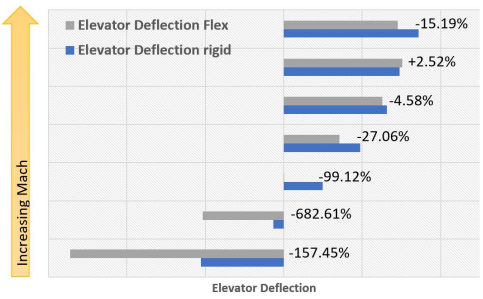

(b) Trim elevator deflection as a variation of Mach number

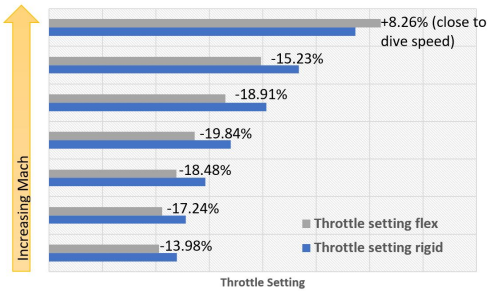

(c) Trim throttle setting as a variation of Mach number

Figure 11: Comparison of rigid and flexible solution at trim for increasing Mach number keeping altitude constant

shows the washout of the wing due to aeroelastic effects at different g's. As expected, the amount of washout increases as the aircraft experiences higher g's.

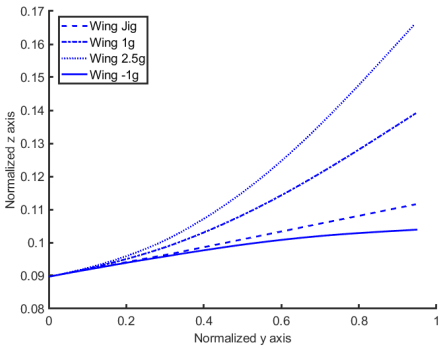

(a) Back view of the aircraft

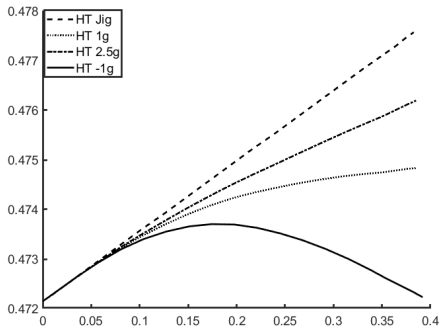

(b) Back view of the aircraft

Figure 12: Deflection at different trimmed g states

VI. Conclusion

In this work, a framework for simulating dynamic maneuvers specified by the Federal Aviation Regulations and obtaining the resulting structural loads was enhanced to account for the effects of structural flexibility. A Timoshenko-like beam structural dynamics model is developed. Time marching can be done to obtain the deformations and the resulting structural loads as a function of time. Aerodynamic forces, being follower forces, contribute terms to the Jacobian of the structural dynamics residual equations. An analytical method

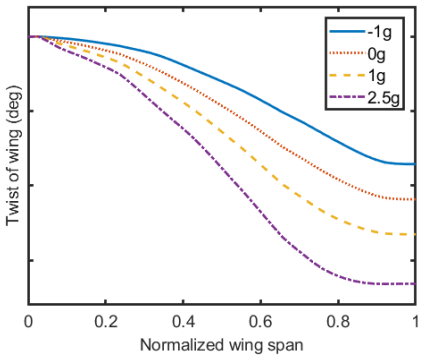

Figure 13: Washout of the wing due to aeroelastic effects at different g's

was presented to obtain the effective angle of attack and sideslip angle at any panel on the beam, and to obtain the partial derivative terms of the Jacobian. The structural dynamics solver along with the aerodynamic build-up are used to obtain trim solution of the aircraft. Results are presented to show how accounting for aeroelasticity affects the trim solution. To perform dynamic maneuvers, the solvers are used inside the Matlab/Simulink framework which integrates the flight dynamics equations of motion forward in time to obtain the time history of the maneuver. Future work will focus on applying the developed approach to more time-domain simulations of maneuvers of interest in order to ascertain the resulting structural loads.

References

[1] National Transportation Safety Board, N. T. S. B., "Aircraft Accident Report NTSB/AAR-04/04," https://www.ntsb.gov/investigations/AccidentReports/Reports/AAR0404.pdf, [Online; accessed 29 October 2017].

[2] Mares, C. and Ursache, N., "Aircraft Ground Structural Testing," *Encyclopedia of Aerospace Engineering*, Vol. 1-16, 2014.

[3] De Florio, F., *Airworthiness: an introduction to aircraft certification*, Elsevier, 2010.

[4] United States Department of Transportation, F. A. A., "Code of Federal Regulations, Title 14, Part 25: Airworthiness Standards: Transport Category Airplanes," https://www.ecfr.gov/cgi-bin/text-idx?SID=c2701f12888e98ced5ba64fa2b0772bb&mc=true&tpl=/ecfrbrowse/Title14/14cfr25_main_02.tpl, [Online; accessed 29 October 2017].

[5] Goron, G., Duca, R., Sarojini, D., Shah, S., Chakraborty, I., Briceno, S., and Mavris, D. N., "A Simulation-Based Framework for Structural Loads Assessment during Dynamic Maneuvers," *AIAA Aviation and Aeronautics Forum and Exposition (AIAA AVIATION Forum) 2017*, Denver, CO, June 5-9, 2017, (AIAA-2017-3767).

[6] Duca, R., Sarojini, D., Blomer, S., Chakraborty, I., Briceno, S., and Mavris, D. N., "Effects of Epistemic Uncertainty on Structural Loads During Dynamic Maneuvers," *AIAA Science and Technology Forum and Exposition (AIAA SciTech Forum) 2018*, Kissimmee, FL, January 8-12, 2018.

[7] "MSC Nastran Multidisciplinary Structural Analysis," http://www.mscsoftware.com/product/msc-nastran, [Online; accessed 29 October 2017].

[8] Seywald, K., *Impact of Aeroelasticity on Flight Dynamics and Handling Qualities of Novel Aircraft Configurations*, Ph.D. thesis, München, Technische Universität München, 2016.

[9] Nguyen, N. T. and Tuzcu, I., "Flight dynamics of flexible aircraft with aeroelastic and inertial force interactions," .

[10] Drela, M., "Integrated simulation model for preliminary aerodynamic, structural, and control-law design of aircraft," *AIAA Paper*, Vol. 99, 1999, pp. 1394.

[11] Drela, M., "ASWING 5.99 Technical Description Steady Formulation," http://web.mit.edu/drela/Public/web/aswing/, 2015.

[12] Drela, M., "ASWING 5.99 Technical Description Unsteady Extension," http://web.mit.edu/drela/Public/web/aswing/, 2015.

[13] "FlightGear flight simulator," http://www.flightgear.org/, [Online; accessed 29 October 2017].

[14] Minguet, P. J., *Static and dynamic behavior of composite helicopter rotor blades under large deflections*, Ph.D. thesis, Massachusetts Institute of Technology, 1989.

VII. Appendix A: Partial Derivatives of Aerodynamic Loads

This appendix provides expressions for the partial derivatives of the aerodynamic loads with respect to structural variables to feed into the Jacobian.

Taking partial derivatives of Equation 43 with respect to the nodal Euler angles ϕ_i, θ_i, ψ_i yields nine partial derivatives:

$$\begin{aligned}
\frac{\partial \Delta r_{p,i,x}}{\partial \phi_i} &= 0 \\
\frac{\partial \Delta r_{p,i,x}}{\partial \theta_i} &= -s_\theta c_\psi \Delta r_{p,i,c} + c_\theta c_\psi \Delta r_{p,i,n} \\
\frac{\partial \Delta r_{p,i,x}}{\partial \psi_i} &= -c_\theta s_\psi \Delta r_{p,i,c} - c_\psi \Delta r_{p,i,s} - s_\theta s_\psi \Delta r_{p,i,n} \\
\frac{\partial \Delta r_{p,i,y}}{\partial \phi_i} &= (-c_\theta s_\psi s_\phi + s_\theta c_\phi)\Delta r_{p,i,c} - c_\psi s_\phi \Delta r_{p,i,s} + (-s_\theta s_\psi s_\phi - c_\theta c_\phi)\Delta r_{p,i,n} \\
\frac{\partial \Delta r_{p,i,y}}{\partial \theta_i} &= (-s_\theta s_\psi c_\phi + c_\theta s_\phi)\Delta r_{p,i,c} + c_\psi c_\phi \Delta r_{p,i,s} + (c_\theta s_\psi c_\phi + s_\theta s_\phi)\Delta r_{p,i,n} \\
\frac{\partial \Delta r_{p,i,y}}{\partial \psi_i} &= (c_\theta c_\psi c_\phi + s_\theta s_\phi)\Delta r_{p,i,c} - s_\psi c_\phi \Delta r_{p,i,s} + (s_\theta c_\psi c_\phi - c_\theta s_\phi)\Delta r_{p,i,n} \\
\frac{\partial \Delta r_{p,i,z}}{\partial \phi_i} &= (c_\theta s_\psi c_\phi + s_\theta s_\phi)\Delta r_{p,i,c} + c_\psi c_\phi \Delta r_{p,i,s} + (s_\theta s_\psi c_\phi - c_\theta s_\phi)\Delta r_{p,i,n} \\
\frac{\partial \Delta r_{p,i,z}}{\partial \theta_i} &= (-s_\theta s_\psi s_\phi - c_\theta c_\phi)\Delta r_{p,i,c} + c_\psi s_\phi \Delta r_{p,i,s} + (c_\theta s_\psi s_\phi - s_\theta c_\phi)\Delta r_{p,i,n} \\
\frac{\partial \Delta r_{p,i,z}}{\partial \psi_i} &= (c_\theta c_\psi s_\phi - s_\theta c_\phi)\Delta r_{p,i,c} - s_\psi s_\phi \Delta r_{p,i,s} + (s_\theta c_\psi s_\phi + c_\theta c_\phi)\Delta r_{p,i,n}
\end{aligned} \tag{52}$$

Let $\lambda = \{U, V, W, P, Q, R, u_i, v_i, w_i, p_i, q_i, r_i, x_i, y_i, z_i, \phi_i, \theta_i, \psi_i\}^T$ denote the quantities with respect to which partial derivatives must be computed analytically to populate the Jacobian. Further, let $\mathcal{F}(\ldots, \alpha_i)$ denote a generalized aerodynamic load (either force or moment) which is a function of nodal incidence angle α_i. Application of chain-rule differentiation yields

$$\frac{\partial \mathcal{F}}{\partial \lambda} = \frac{\partial \mathcal{F}}{\partial \alpha_i} \cdot \frac{\partial \alpha_i}{\partial \lambda} = \frac{\partial \mathcal{F}}{\partial \alpha_i} \cdot \frac{1}{1 + (V_{p,i,n}/V_{p,i,c})^2} \cdot \frac{V_{p,i,c}\frac{\partial V_{p,i,n}}{\partial \lambda} - V_{p,i,n}\frac{\partial V_{p,i,c}}{\partial \lambda}}{V_{p,i,c}^2} \tag{53}$$

In Equation 53, the quantity $\frac{\partial \mathcal{F}}{\partial \alpha_i}$ can be evaluated by finite differencing from the aerodynamic tables. Analytical expressions follow for the remaining partial derivatives $\frac{\partial V_{p,i,n}}{\partial \lambda}$ and $\frac{\partial V_{p,i,c}}{\partial \lambda}$.

VII..1. Partial derivatives of chordwise velocity $V_{p,i,c}$

The partial derivatives of the chordwise velocity $V_{p,i,c}$ at the i'th node with respect to the elements of λ are given by:

$$
\begin{aligned}
\frac{\partial V_{p,i,c}}{\partial U} &= \frac{\partial V_{p,i,c}}{\partial u_i} = c_\theta c_\psi \\
\frac{\partial V_{p,i,c}}{\partial V} &= \frac{\partial V_{p,i,c}}{\partial v_i} = c_\theta s_\psi c_\phi + s_\theta s_\phi \\
\frac{\partial V_{p,i,c}}{\partial W} &= \frac{\partial V_{p,i,c}}{\partial w_i} = c_\theta s_\psi s_\phi - s_\theta c_\phi \\
\frac{\partial V_{p,i,c}}{\partial P} &= \frac{\partial V_{p,i,c}}{\partial p_i} = (c_\theta s_\psi c_\phi + s_\theta s_\phi)(-z_i - \Delta r_{p,i,z}) + (c_\theta s_\psi s_\phi - s_\theta c_\phi)(y_i + \Delta r_{p,i,y}) \\
\frac{\partial V_{p,i,c}}{\partial Q} &= \frac{\partial V_{p,i,c}}{\partial q_i} = c_\theta c_\psi (z_i + \Delta r_{p,i,z}) + (c_\theta s_\psi s_\phi - s_\theta c_\phi)(-x_i - \Delta r_{p,i,x}) \\
\frac{\partial V_{p,i,c}}{\partial R} &= \frac{\partial V_{p,i,c}}{\partial r_i} = c_\theta c_\psi (-y_i - \Delta r_{p,i,y}) + (c_\theta s_\psi c_\phi + s_\theta s_\phi)(x_i + \Delta r_{p,i,x}) \\
\frac{\partial V_{p,i,c}}{\partial x_i} &= R(c_\theta s_\psi c_\phi + s_\theta s_\phi) - Q(c_\theta s_\psi s_\phi - s_\theta c_\phi) \\
\frac{\partial V_{p,i,c}}{\partial y_i} &= -R c_\theta c_\psi + P(c_\theta s_\psi s_\phi - s_\theta c_\phi) \\
\frac{\partial V_{p,i,c}}{\partial z_i} &= Q c_\theta c_\psi - P(c_\theta s_\psi c_\phi + s_\theta s_\phi) \\
\frac{\partial V_{p,i,c}}{\partial \phi_i} &= (-c_\theta s_\psi s_\phi + s_\theta c_\phi) V_{p,i,y} + (c_\theta s_\psi c_\phi + s_\theta s_\phi) V_{p,i,z} \\
&+ c_\theta c_\psi \left(-(R + r_i) \frac{\partial \Delta r_{p,i,y}}{\partial \phi_i} + (Q + q_i) \frac{\partial \Delta r_{p,i,z}}{\partial \phi_i} \right) \\
&+ (c_\theta s_\psi c_\phi + s_\theta s_\phi) \left((R + r_i) \frac{\partial \Delta r_{p,i,x}}{\partial \phi_i} - (P + p_i) \frac{\partial \Delta r_{p,i,z}}{\partial \phi_i} \right) \\
&+ (c_\theta s_\psi s_\phi - s_\theta c_\phi) \left(-(Q + q_i) \frac{\partial \Delta r_{p,i,x}}{\partial \phi_i} + (P + p_i) \frac{\partial \Delta r_{p,i,y}}{\partial \phi_i} \right) \\
\frac{\partial V_{p,i,c}}{\partial \theta_i} &= -s_\theta c_\psi V_{p,i,x} + (-s_\theta s_\psi c_\phi + c_\theta s_\phi) V_{p,i,y} + (-s_\theta s_\psi s_\phi - c_\theta c_\phi) V_{p,i,z} \\
&+ c_\theta c_\psi \left(-(R + r_i) \frac{\partial \Delta r_{p,i,y}}{\partial \theta_i} + (Q + q_i) \frac{\partial \Delta r_{p,i,z}}{\partial \theta_i} \right) \\
&+ (c_\theta s_\psi c_\phi + s_\theta s_\phi) \left((R + r_i) \frac{\partial \Delta r_{p,i,x}}{\partial \theta_i} - (P + p_i) \frac{\partial \Delta r_{p,i,z}}{\partial \theta_i} \right) \\
&+ (c_\theta s_\psi s_\phi - s_\theta c_\phi) \left(-(Q + q_i) \frac{\partial \Delta r_{p,i,x}}{\partial \theta_i} + (P + p_i) \frac{\partial \Delta r_{p,i,y}}{\partial \theta_i} \right) \\
\frac{\partial V_{p,i,c}}{\partial \psi_i} &= -c_\theta s_\psi V_{p,i,x} + (c_\theta c_\psi c_\phi + s_\theta s_\phi) V_{p,i,y} + (c_\theta c_\psi s_\phi - s_\theta c_\phi) V_{p,i,z} \\
&+ c_\theta c_\psi \left(-(R + r_i) \frac{\partial \Delta r_{p,i,y}}{\partial \psi_i} + (Q + q_i) \frac{\partial \Delta r_{p,i,z}}{\partial \psi_i} \right) \\
&+ (c_\theta s_\psi c_\phi + s_\theta s_\phi) \left((R + r_i) \frac{\partial \Delta r_{p,i,x}}{\partial \psi_i} - (P + p_i) \frac{\partial \Delta r_{p,i,z}}{\partial \psi_i} \right) \\
&+ (c_\theta s_\psi s_\phi - s_\theta c_\phi) \left(-(Q + q_i) \frac{\partial \Delta r_{p,i,x}}{\partial \psi_i} + (P + p_i) \frac{\partial \Delta r_{p,i,y}}{\partial \psi_i} \right)
\end{aligned}
\tag{54}
$$

Note that analytical expressions for the partial derivatives occurring in the RHS of Equation 54 have been obtained in Equation 52.

VII..2. Partial derivatives of normal velocity $V_{p,i,n}$

The partial derivatives of the normal velocity $V_{n,i,c}$ at the i'th node with respect to the elements of λ are given by:

$$
\begin{aligned}
\frac{\partial V_{p,i,n}}{\partial U} &= \frac{\partial V_{p,i,n}}{\partial u_i} = s_\theta c_\psi \\
\frac{\partial V_{p,i,n}}{\partial V} &= \frac{\partial V_{p,i,n}}{\partial v_i} = s_\theta s_\psi c_\phi - c_\theta s_\phi \\
\frac{\partial V_{p,i,n}}{\partial W} &= \frac{\partial V_{p,i,n}}{\partial w_i} = s_\theta s_\psi s_\phi + c_\theta c_\phi \\
\frac{\partial V_{p,i,n}}{\partial P} &= \frac{\partial V_{p,i,n}}{\partial p_i} = (s_\theta s_\psi c_\phi - c_\theta s_\phi)(-z_i - \Delta r_{p,i,z}) + (s_\theta s_\psi s_\phi + c_\theta c_\phi)(y_i + \Delta r_{p,i,y}) \\
\frac{\partial V_{p,i,n}}{\partial Q} &= \frac{\partial V_{p,i,n}}{\partial q_i} = s_\theta c_\psi (z_i + \Delta r_{p,i,z}) + (s_\theta s_\psi s_\phi + c_\theta c_\phi)(-x_i - \Delta r_{p,i,x}) \\
\frac{\partial V_{p,i,n}}{\partial R} &= \frac{\partial V_{p,i,n}}{\partial r_i} = s_\theta c_\psi (-y_i - \Delta r_{p,i,y}) + (s_\theta s_\psi c_\phi - c_\theta s_\phi)(x_i + \Delta r_{p,i,x}) \\
\frac{\partial V_{p,i,n}}{\partial x_i} &= R(s_\theta s_\psi c_\phi - c_\theta s_\phi) - Q(s_\theta s_\psi s_\phi + c_\theta c_\phi) \\
\frac{\partial V_{p,i,n}}{\partial y_i} &= -R s_\theta c_\psi + P(s_\theta s_\psi s_\phi + c_\theta c_\phi) \\
\frac{\partial V_{p,i,n}}{\partial z_i} &= Q s_\theta c_\psi V_{p,i,x} - P(s_\theta s_\psi c_\phi - c_\theta s_\phi) \\
\frac{\partial V_{p,i,n}}{\partial \phi_i} &= (-s_\theta s_\psi s_\phi - c_\theta c_\phi) V_{p,i,y} + (s_\theta s_\psi c_\phi - c_\theta s_\phi) V_{p,i,z} \\
&+ s_\theta c_\psi \left(-(R + r_i) \frac{\partial \Delta r_{p,i,y}}{\partial \phi_i} + (Q + q_i) \frac{\partial \Delta r_{p,i,z}}{\partial \phi_i} \right) \\
&+ (s_\theta s_\psi c_\phi - c_\theta s_\phi) \left((R + r_i) \frac{\partial \Delta r_{p,i,x}}{\partial \phi_i} - (P + p_i) \frac{\partial \Delta r_{p,i,z}}{\partial \phi_i} \right) \\
&+ (s_\theta s_\psi s_\phi + c_\theta c_\phi) \left(-(Q + q_i) \frac{\partial \Delta r_{p,i,x}}{\partial \phi_i} + (P + p_i) \frac{\partial \Delta r_{p,i,y}}{\partial \phi_i} \right) \\
\frac{\partial V_{p,i,n}}{\partial \theta_i} &= c_\theta c_\psi V_{p,i,x} + (c_\theta s_\psi c_\phi + s_\theta s_\phi) V_{p,i,y} + (c_\theta s_\psi s_\phi - s_\theta c_\phi) V_{p,i,z} \\
&+ s_\theta c_\psi \left(-(R + r_i) \frac{\partial \Delta r_{p,i,y}}{\partial \theta_i} + (Q + q_i) \frac{\partial \Delta r_{p,i,z}}{\partial \theta_i} \right) \\
&+ (s_\theta s_\psi c_\phi - c_\theta s_\phi) \left((R + r_i) \frac{\partial \Delta r_{p,i,x}}{\partial \theta_i} - (P + p_i) \frac{\partial \Delta r_{p,i,z}}{\partial \theta_i} \right) \\
&+ (s_\theta s_\psi s_\phi + c_\theta c_\phi) \left(-(Q + q_i) \frac{\partial \Delta r_{p,i,x}}{\partial \theta_i} + (P + p_i) \frac{\partial \Delta r_{p,i,y}}{\partial \theta_i} \right) \\
\frac{\partial V_{p,i,n}}{\partial \psi_i} &= -s_\theta s_\psi V_{p,i,x} + (s_\theta c_\psi c_\phi - c_\theta s_\phi) V_{p,i,y} + (s_\theta c_\psi s_\phi + c_\theta c_\phi) V_{p,i,z} \\
&+ s_\theta c_\psi \left(-(R + r_i) \frac{\partial \Delta r_{p,i,y}}{\partial \psi_i} + (Q + q_i) \frac{\partial \Delta r_{p,i,z}}{\partial \psi_i} \right) \\
&+ (s_\theta s_\psi c_\phi - c_\theta s_\phi) \left((R + r_i) \frac{\partial \Delta r_{p,i,x}}{\partial \psi_i} - (P + p_i) \frac{\partial \Delta r_{p,i,z}}{\partial \psi_i} \right) \\
&+ (s_\theta s_\psi s_\phi + c_\theta c_\psi) \left(-(Q + q_i) \frac{\partial \Delta r_{p,i,x}}{\partial \psi_i} + (P + p_i) \frac{\partial \Delta r_{p,i,y}}{\partial \psi_i} \right)
\end{aligned}
\tag{55}
$$

Note that analytical expressions for the partial derivatives occurring in the RHS of Equation 54 have been obtained in Equation 52.